applied sciences

MDPI

Article

Bayesian Assessment of the Effects of Cyclic Loads on the Chloride Ingress Process into Reinforced Concrete

Henriette Marlaine Imounga [1,2], Emilio Bastidas-Arteaga [1,*], Rostand Moutou Pitti [3,4], Serge Ekomy Ango [4] and Xiao-Hui Wang [5]

1 Institute for Research in Civil and Mechanical Engineering, University of Nantes, CNRS UMR 6183, BP 92208, 44000 Nantes, France; henriette.imounga@etu.univ-nantes.fr
2 University of Science and Technology of Masuku, BP 941, Franceville 14810, Gabon
3 Institute Pascal, University Clermont Auvergne, CNRS, SIGMA Clermont, 63000 Clermont Ferrand, France; rostand.moutou_pitti@uca.fr
4 Institute for Technological Research, CENAREST, BP, Libreville 14070, Gabon; ekomyango@yahoo.fr
5 College of Ocean Science and Engineering, Shanghai Maritime University, Shanghai 201306, China; w_xiaoh@163.com
* Correspondence: emilio.bastidas@univ-nantes.fr; Tel.: +33-2-51-12-55-24

Received: 7 February 2020; Accepted: 10 March 2020; Published: 17 March 2020

Abstract: Chloride-induced corrosion and load induced concrete cracking affect the serviceability and safety of reinforced concrete (RC) structures. Once these phenomena occur simultaneously, the prediction of RC structures' lifetimes becomes a major challenge. The objective of this paper is to propose a methodology to evaluate the effect of loading and cracking on the mechanism of chloride ion penetration in concrete. The proposed methodology will be based on Bayesian networks. Bayesian networks are useful to update the lifetime assessment based on experimental data as well as to characterize the uncertainties of the input parameters of a chlorination model including a chloride diffusion acceleration factor. The proposed methodology is illustrated with experimental data coming from tests on RC beams subjected to static and cyclic loading before being in contact with a solution containing chloride ions. The characterized parameters are then used to evaluate the effect of these two loading conditions (static and cyclic) on the corrosion initiation time and the corrosion initiation probability. The results obtained indicate that the proposed methodology is capable of integrating loading and chlorination test data for the determination of the probabilistic parameters of a model in a comprehensive way.

Keywords: bayesian networks; chlorination; reinforced concrete; cyclic loading; corrosion; cracking

1. Introduction

Reinforced concrete (RC) is a resistant and durable material that is widely used in the construction of different types of structure. It is one of the most used materials in the world because of the availability of its components and its ease of construction. However, structures placed in coastal and offshore areas are exposed to chloride-induced corrosion. The penetration of chloride ions is one of the major causes of deterioration of RC structures [1,2]. It causes a local reduction in the reinforcement and an accumulation of corrosion products at the interface between concrete and steel, which lead to tensile stresses that initiate cracks. The different effects of chloride-induced corrosion produce a significant reduction in the service life and structural safety, as well as an increase of maintenance costs [3–5]. Reinforced concrete structures, generally designed for a lifetime of 50 to 100 years, could begin to deteriorate after 20 to 30 years when are in contact with chloride ions [6–8]. In addition, structures in service are subject to mechanical stresses such as cyclic loads, which cause cracks in the reinforced

concrete. This cracking modifies the porous structure of the concrete and, therefore, modify the chloride ion-diffusion process [4,9,10].

Cracks and defects in concrete elements are detected and characterized using destructive or non-destructive testing (NDT) methods. Destructive inspection techniques are restrictive to be used in situ and they are expensive, unlike NDT, which are inexpensive, efficient and more suitable for reinforced-concrete structures [11]. Acoustic emission (AE) and digital image correlation (DIC) are among the most frequently used NDT methods. For example, Golewski [12] applied the DIC method to measure the displacement, deformation and development of cracks continuously on concrete slabs containing fly ash. This study shows the usefulness of DIC for the precise determination of the parameters of the fracture mechanics in concrete composites. Niewiadomski et al. [13] used the AE method to characterize the failure parameters of a self-compacting concrete modified with the addition of nanoparticles of SiO_2 and TiO_2. Non-destructive methods have also been applied individually, or in a combined way, in many studies to determine unknown material properties and defects [11,14,15].

This paper focuses on the chloride ingress into concrete considering the effects of static and cyclic loading. Corrosion and cracking are two of the main causes of degradation of reinforced or prestressed concrete structures. For structures placed in corrosive environments and subjected to complex loads (for example bridges, offshore wind turbines, etc.), there is an interaction between chloride-induced corrosion and concrete cracking due to loadings. Indeed, the products of corrosion increase the number of cracks [16–18], and cracks induced by loading increase the amount of chloride in concrete [4,9,18]. Therefore, the coupling of these two phenomena accelerates the deterioration of structures, thus reducing their resistance and lifetime [4,17].

Several authors have worked on the coupled effects of corrosion and cyclic load in RC structures. Giordano et al. [19] conducted an experimental campaign to evaluate the combined effects of accelerated corrosion and mechanical actions (cyclic loading, and cyclic and static loading) on concrete beams. The results showed that the evolution of longitudinal cracks in concrete due to corrosion depends on the level and type of the load. Other authors [20,21] evaluated the durability of RC structures subjected to the combined effects of corrosion and loading-induced cracking. These studies have shown that mechanical loadings significantly reduce the time and probability of initiation of corrosion depending on the exposure conditions.

The diffusion of chlorides into concrete is a complex phenomenon where chemical and physical mechanisms interact depending on material properties and environmental exposure. Therefore, there are several sources of uncertainty related to chloride ingress modeling. According to Saassouh and Lounis [22], these uncertainties may come from not only the key parameters of the model (concrete cover depth, chloride concentration at the surface, diffusion coefficient, chloride threshold concentration) but also from the models (physical and surrogate), and measurement methods chosen. Consequently, probabilistic models that take into account the uncertainty and variability of the main parameters are more suitable for lifetime assessment [23–25]. These models also allow prediction of the probability of corrosion of the rebars and its sensitivity to the different parameters. Bastidas-Arteaga et al. [16] proposed a probabilistic model of fatigue corrosion for RC structures. This model combined a simple solution of Fick's law [26], electrochemical principles, a rate competition Criterion and linear elastic fracture mechanics. It was updated recently [17] to account for a more realistic model of chloride ingress; but it still neglects the effects of loading on the chloride ingress process. Characterizing the effects of loading on the chloride ingress mechanism is a major challenge that should be addressed to improve the lifetime assessment for in-service RC structures.

In this context, the main objective of this work is to propose a methodology for the probabilistic characterization of the input parameters of a chlorination model taking into account the effects of loading. The proposed methodology is based on the Bayesian network (BN) approach, which is a probabilistic tool that could be used to identify parameters by integrating experimental data. The Bayesian approach has already been used to update/identify the parameters of chlorination models, and to assess/update the reliability of concrete [27,28] or timber [29,30] structures. However, it has not

been used to estimate the effects of mechanical loading on the chloride ingress mechanism by using experimental data. The experimental data presented in the paper comes from a previous research study on the combined effects of chlorination and cracking detailed in [4].

The paper is organized as follows. The first part of the document summarizes the chloride diffusion models in sound and cracked concrete (Section 2). Section 3 gives a general description of the experimental tests by presenting the equipment, method and inspection data that will be used for identification purposes. In Section 4, we detail the proposed Bayesian network that will be used to characterize the model parameters. Finally, Section 5 deals with the results of the identification of input variables for different loading cases and their effects the probability of corrosion initiation.

2. Chloride Ingress Modeling

2.1. Chloride Ingress for Uncracked Concrete

The diffusion of chloride ions in saturated concretes is described by the second Fick's law [26] with the assumption that concrete is a homogeneous and isotropic material [31]:

$$\frac{\partial C}{\partial t} = D\frac{\partial^2 C}{\partial x^2} \tag{1}$$

where C is the free chloride concentration, t is time, D is the diffusion coefficient of the chloride ions, and x is the depth of the concrete in the diffusion direction. With the following initial conditions: (1) the concentration is zero at the beginning of the exposure t_0, and (2) the chloride surface concentration is constant; the concentration of free chloride ions $C(x,t)$ at depth x and at time t for a semi-infinite medium can be expressed by an analytical solution of Fick law using the error function:

$$C(x,t) = C_s\left[1 - \mathrm{erf}\left(\frac{x}{2\sqrt{D\cdot t}}\right)\right] \tag{2}$$

where C_s is the chloride concentration at the surface, and $\mathrm{erf}(\cdot)$ is the error function. This solution makes possible to calculate chloride profiles at given times and depths as well as the corrosion initiation time t_{ini}. t_{ini} is the time at which the chloride concentration at the surface of the reinforcements reaches a threshold value C_{th}. This threshold value represents the concentration of chlorides for which the passive layer of the steel is destroyed and the corrosion reaction starts. The corrosion initiation time is, therefore, estimated for the chloride concentration equal to the threshold value C_{th} and x equal to the cover depth of the concrete c, according to the following equation:

$$t_{ini} = \frac{c^2}{4D}\left[\mathrm{erf}^{-1}\left(1 - \frac{C_{th}}{C_s}\right)\right]^{-2} \tag{3}$$

Collepardi's model (Equation (2)) is only valid for saturated concrete exposed to a constant concentration of chloride on the surface. In reality, for a heterogeneous material, such as concrete, these conditions are rarely observed and the concentration of chlorides on the surface varies over time. Although this model does not take into account several important parameters such as the aging state of concrete and environmental factors (temperature, humidity) [32,33], it will be used to identify the variables required because the beams of the tests are subjected to a constant concentration of chloride on the surface of the concrete. In addition, this solution (Equation (2)) remains complex enough to illustrate the proposed methodology. More elaborated models could be considered but they require additional experimental data to determine supplementary model parameters.

2.2. Chloride Ingress for Cracked Concrete

In recent years, much research has been devoted to the development of models for predicting the cracking effects on chloride ingress and corrosion phenomenon (corrosion initiation, propagation,

corrosion rate, etc.). Otieno et al. [34] have developed empirical models for predicting the rate of corrosion induced by chloride ions in cracked RC structures. These models incorporated the influence of several geometries of concrete cracks and cover depth (with the crack width/concrete cover ratio [35,36]), as well as the quality of concrete on the corrosion speed. This study was useful to provide recommendations about the best combination of the aforementioned parameters to meet the desired durability performance of the structure. Kurumatani et al. [37] have proposed a numerical method that allowed simulating the chloride ingress into concrete by an unstable diffusion analysis, taking into account damage associated with 3D internal cracks. The crack propagation analysis with a damage model based on fracture mechanics was also taken into account to reproduce the 3D geometry of the internal cracks. Several authors have also developed models of corrosion or chloride transport into cracked concrete (saturated or unsaturated) at the mesoscale, to consider the heterogeneity of concrete in more than two phases [38–40].

Several experiments as well as field studies have shown that cracking leads to rapid penetration of chloride ions and early degradation of structures [41–43]. For example, Gowripalan et al. [35] conducted chloride diffusing tests on cracked RC beams, and concluded that the crack width/concrete cover ratio may be a deterministic parameter for assessing the durability of cracked reinforced concrete. His research has shown that there is a hyperbolic relationship between this ratio and the chloride threshold value in cracked concrete. The introduction of cracking parameters in chlorination models is therefore useful for estimating the time of corrosion initiation taking into account the combined effects of chloride ingress and concrete cracking. To model the diffusion of chlorides in cracked concrete, we propose to use the simplified model described by Equation (4) in which we add an acceleration factor α which multiplies the diffusion coefficient D:

$$C(x,t) = C_s\left[1 - \mathrm{erf}\left(\frac{x}{2\sqrt{\alpha \cdot D \cdot t}}\right)\right] \quad (4)$$

The acceleration factor is higher than 1 for cracked conditions to consider that major chloride diffusion is expected in a cracked concrete. Since there are significant uncertainties related to this parameter depending on the concrete properties, fabrication of the structural component, loading history, etc. this parameter should be modeled as a random variable to be identified from experimental data.

3. Tests' Description

3.1. General Description

The tests were carried out on 12 RC beams (300 × 120 × 1500 mm, Figure 1), designed according to Chinese standards GB/T 50081-2016 [44]. The different stages of the experimental tests are presented in the form of a flowchart in Figure 2 (for more details see [4]). Stage I includes the fabrication and curing (28 days) of the reinforced concrete specimens. RC specimens have made from commercial concrete with a target strength of 40 MPa at 28 days and a water/cement ratio 0.44 chosen according requirements of [45] for the concrete elements in a chloride-containing environment. The composition and additional details of concrete are provided in Table 1.

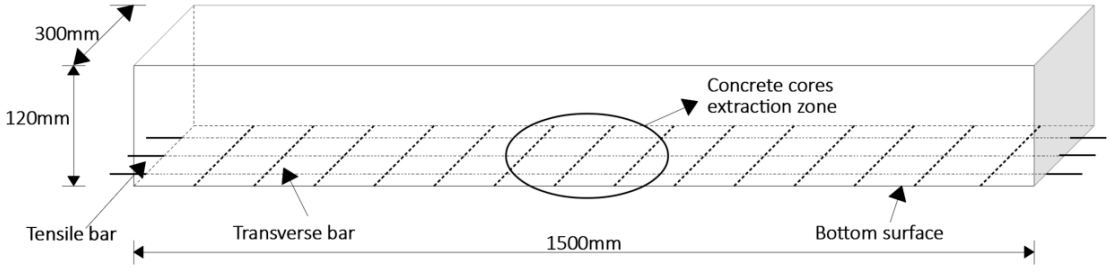

Figure 1. Reinforced-concrete test specimen.

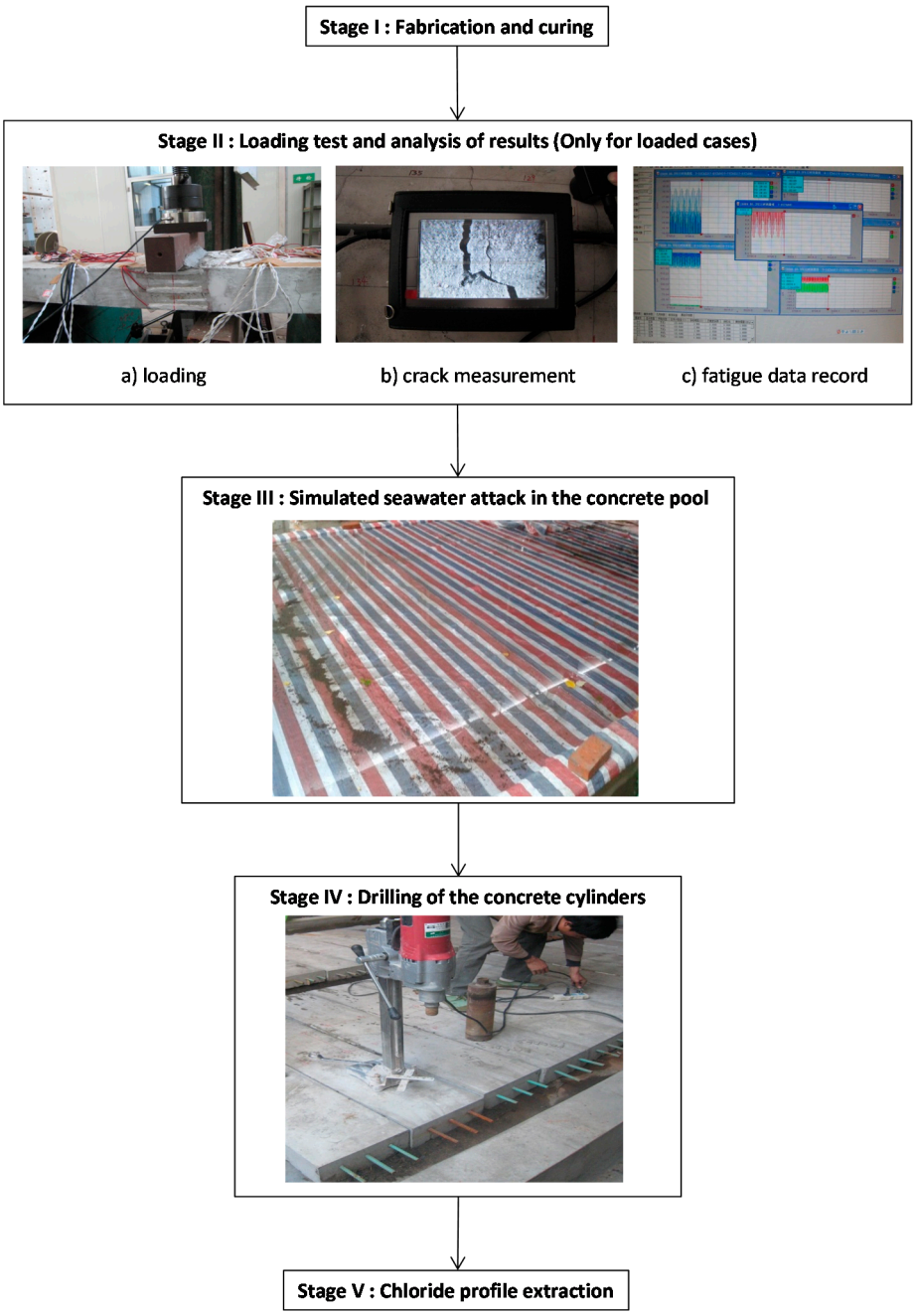

Figure 2. Stages of experimental tests.

Table 1. Characteristics of the concrete mixture [4].

Target Concrete Strength			C40 MPa
Materials and Mix Proportion		Water (tape water)	180 kg/m^3
		Cement (PII 52.5)	320 kg/m^3
		Furnace micro-slag (S95)	90 kg/m^3
	Aggregates	Fine aggregates (middle size)	770 kg/m^3
		Coarse aggregates (5–25 mm, crushed)	1020 kg/m^3
		Super plasticizer (LN800)	4.51 kg/m^3
Properties		Slump (mm)	140 ± 20 mm
		28-day compressive strength 150 × 150 × 150 mm concrete cube (MPa)	50.0 MPa

In stage II (Figure 2), the specimens were subjected to no loading (4 beams), static loads (single load of 18 kN, 4 beams) and cyclic loads (500,000 loading cycles 5.4k N to 18 kN, 4 beams) using a three-point loading test. The control and record of static and cyclic load magnitudes were carried out by a load cell [46].

After the mechanical tests, the beams were exposed to chloride ions by wetting and immerging the beams in a 3.5%~5% NaCl solution (Stage III in Figure 2). The beams were first covered with a sponge wetted with 3.5%~5% NaCl solution and dried. Afterwards, they were completely immersed in a pool filled with this same solution and dried. A total of four wetting/drying cycles and three immersion/drying cycles were performed during 388 days [47].

Once the chloride exposures were completed, four cylinders (100 mm diameter × 120 mm height) were drilled in the center zone of each beam (Stage IV in Figure 2). In Stage V, the cylinders were cut in 10 mm slices. These slices were oven dried and ground to powder to make a complete blend [4]. The resulting powders were used to measure the total content of concrete chlorides at four depths (5 mm, 15 mm, 25 mm and 35 mm). Three categories of tests were studied according to the loading conditions: uncharged tests, static and cyclic loading. In total, 12 chloride profiles were measured for each category.

3.2. Test Results

The results of the tests presented in this section will be used to illustrate the developed methodology for the identification purposes. After the loading tests, the maximum width of the crack varied between 0.15 and 0.25 mm for the cyclic load case, and between 0.04 and 0.06 mm for static load case. The results of the chloride measurements in the concrete as a function of the depth for each load case are detailed in Appendix A (Tables A1–A3).

Based on these experimental data, Wang et al. [4] estimated the input parameters of a simple chloride diffusion model (Collepardi's model [26,31]). These parameters are the concentration of chloride ions at the surface C_s and the chloride diffusion coefficient D. The results of the study given in the following section presents the models of chloride ion diffusion in the sound (uncracked) and cracked concrete considered in this work.

Table 2 showed that the loadings increase the values identified for the mean and the standard deviation of these parameters compared to the unloaded state. Therefore, we propose in the following section a procedure based on Bayesian networks that could be used towards this aim.

Table 2. Mean and standard deviation of chloride ingress model parameters for different loading conditions.

Case	Mean C_s (% Cl^-)	Standard Deviation C_s (% Cl^-)	Mean D (mm^2/day)	Standard Deviation D (mm^2/day)
Unloaded	0.28	0.05	0.94	0.52
Static load	0.27	0.06	1.31	0.60
Cyclic load	0.30	0.05	1.65	0.77

4. Modeling and Implementation

4.1. Basics of Bayesian Networks

A Bayesian network is the graphical representation of the influence of one event, one fact, or one variable on another. It is a directed acyclic graph (DAG) composed of parent and child nodes (existing real events) modeled as random variables, and oriented arrows that represent the causal relationship

between the nodes. To each child node is associated a conditional probability with respect to its parent node and the set of nodes is defined on the probabilized space ($\boldsymbol{\Omega}$, $\mathbf{X}$) such that:

$$P(\mathbf{X}) = P(X_1, \ldots, X_N) = \prod_{i=1}^{N} P\left(X_i \left| pa\left(X_i\right)\right.\right) \quad (5)$$

where $\boldsymbol{\Omega}$ is the samples space, $\mathbf{X}$ is the set of random variables $\{X_1, \ldots, X_N\}$, and $pa(X_i)$ is the set of parents of the X_i nodes (for more information see [48]). Figure 3 illustrates a simple three-node Bayesian network corresponding to three random variables Y, X_1, and X_2 where X_1 and X_2 are the child nodes of the parent node Y. The joint probability of the events (Y, X_1, X_2) of this network is given as the product of conditional probabilities:

$$P(Y, X_1, X_2) = P(X_1|Y)P(X_2|Y)P(Y) \quad (6)$$

where $P(X_i|Y)$ is the conditional probability of X_i knowing Y.

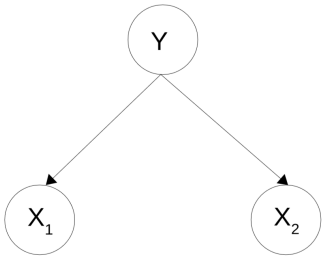

Figure 3. A simple Bayesian network.

Bayesian networks are useful to update probabilities in the network by integrating new information of observed variables called evidences. In our study, the methodology will allow us to integrate information from experimental trials to characterize random variables.

4.2. Numerical Implementation

4.2.1. Proposed Bayesian Network Configuration for Random Variable Characterization

The proposed configuration of the Bayesian network will depend on the loading conditions of the tests. In this case, we have two configurations depending on whether the beam is loaded or unloaded (Figure 4). The input parameters to be determined C_s, D and α are modeled as parent nodes of the Bayesian networks according to the loading case. The child nodes represent the chloride profiles at the four measurement depths of $C(x_i, t)$) and are the same for all loading conditions: x_i = 5 mm, 15 mm, 25 mm and 35 mm) in both cases. All inspections are undertaken at the same time after exposure t = 388 days. For tests without load, we observe in Figure 4 that we have six nodes including two parent nodes (C_s and D) and four child nodes ($C(x_1, t)$, $C(x_2, t)$, $C(x_3, t)$ and $C(x_4, t)$). For tests with load (static or cyclic), the parameter α is added as a parent node giving seven nodes for this network (Figure 4).

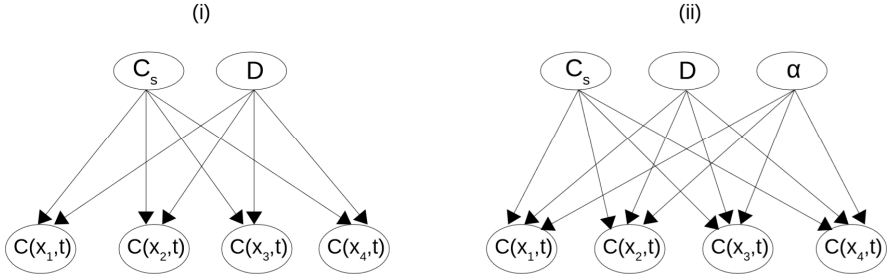

Figure 4. Bayesian networks setup for (**i**) unloaded and (**ii**) loaded conditions.

We consider that all the nodes are discrete and independent. All nodes are divided into a number of states in a range whose boundaries were chosen large enough to cover most possible values of the different nodes. As the observed data are limited, the number of states has been adjusted to get more accurate results. The details of the discretization and the prior information of the different nodes are summarized in Table 3; Table 4 for unloaded and loaded conditions, respectively. The a priori distributions of parent nodes were modeled as uniform distributions for the Bayesian network under unloaded conditions and the acceleration factor α for the Bayesian network under loaded conditions. With the uniform distribution, there is any assumption on the a priori shape of these parameters in order to obtain not skewed results after the characterization process. The a posteriori outputs (histograms) of C_s and D for the Bayesian network under unloaded conditions are used as a priori distributions for these parameters in the Bayesian network under loaded conditions (Table 4). This procedure is justified in Section 4.2.2.

Table 3. Discretization of nodes and a priori information for the Bayesian network under unloaded conditions.

Parameters	Number of States	A Priori Distribution	Boundaries
C_s (% Cl^-)	50	Uniform	[0; 2]
D (mm^2/day)	50	Uniform	[10^{-12}; 4]
$C(x_i, t)$ (% Cl^-)	60	-	[0; 2]

Table 4. Discretization of nodes and a priori information for the Bayesian network under loaded conditions.

Parameters	Number of States	A Priori Distribution	Boundaries
C_s (% Cl^-)	50	Obtained from a posteriori histograms	[0; 2]
D (mm^2/day)	50	Unloading test histogram	[10^{-12}; 4]
α	50	Uniform	[1; 6]
$C(x_i, t)$ (% Cl^-)	60	-	[0; 2]

4.2.2. Proposed Characterization Methodology

The proposed methodology for characterizing the different parameters (C_s, D and α) is illustrated in Figure 5. The Bayesian networks shown in Figure 4 allow us to integrate the observed information on the child nodes (chloride measurements at different depths) in order to update the a posteriori probabilities of their parent nodes. The proposed methodology is composed by two steps, the first one aims at determining C_s and D from unloading test data. It is supposed that the parameters identified during this step are representative of the exposure conditions (i.e., C_s) and chloride diffusivity (i.e., D) for uncracked concrete. The factor α is identified in Step 2 using the evidence of tests with loading (static or cyclic). The a posteriori histograms of C_s and D in Step 1 are used as prior information of Step 2. This procedure allows us to focus the characterization process on the acceleration factor α. At the end of each step, a posteriori histograms of the variables are used to characterize the distribution, mean and standard deviation of each parent node.

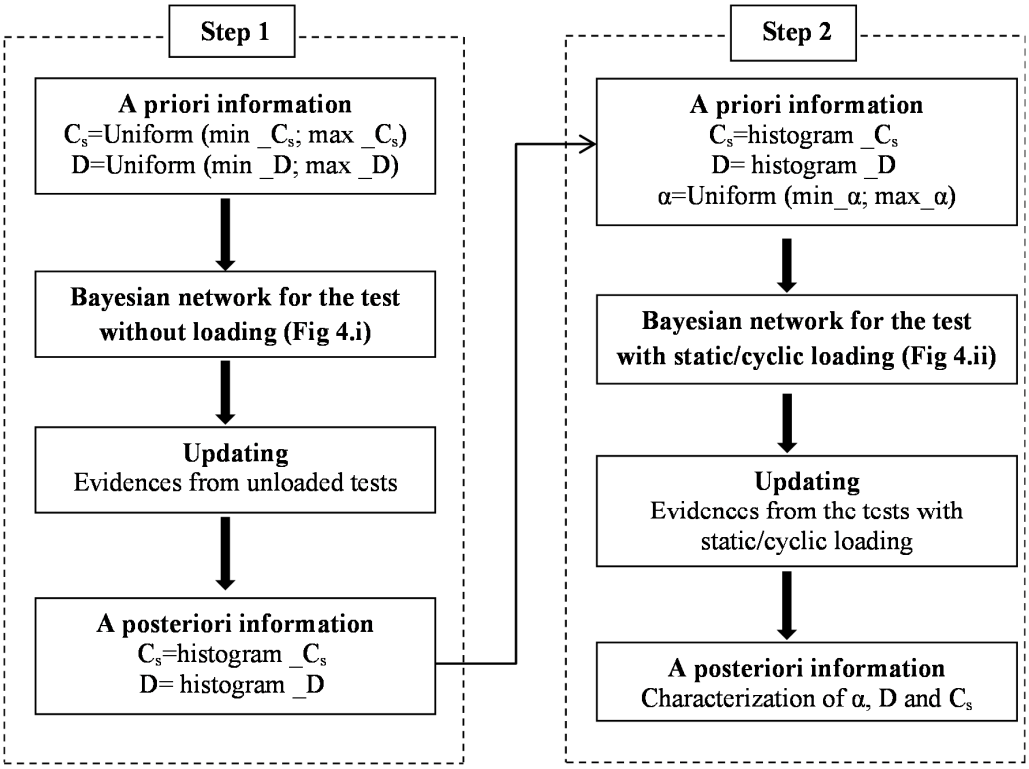

Figure 5. Flowchart of the proposed methodology.

5. Results and Discussion

The objective of this section is to apply the proposed methodology to evaluate and quantify the effect of loading on the chloride ingress mechanism. In Section 5.1, we present and discuss the results of the characterization of the input parameters of the chloride ingress model. The identified values are then used to calculate the time and probability of corrosion initiation in Section 5.2.

5.1. Parameter Characterization

The output histograms of C_s, D, and α are also updated after each step of the procedure (Figures 6–8, respectively). The changes in Figures 6 and 7 after updating are due to the fact that in Step 2 we have added additional information on these two parameters for the loaded tests. These a posteriori histograms will be used to characterize the mean and standard deviation of the model parameters by considering loading conditions.

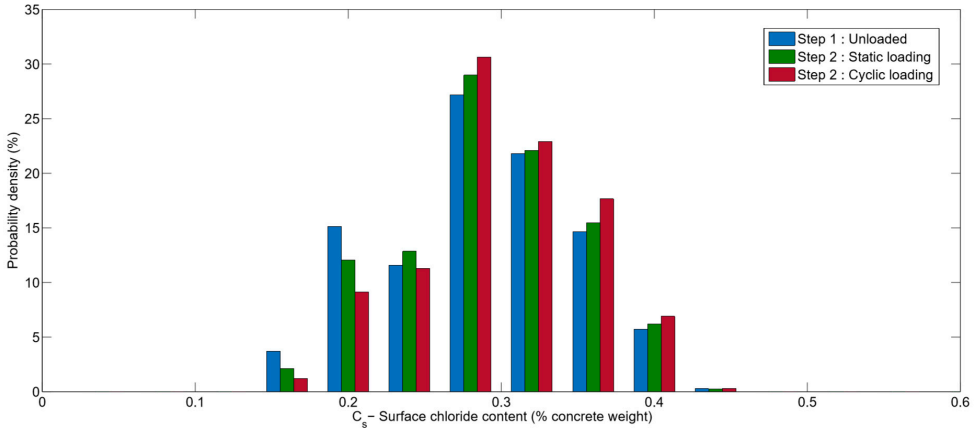

Figure 6. Comparison of a priori and a posteriori histograms of C_s.

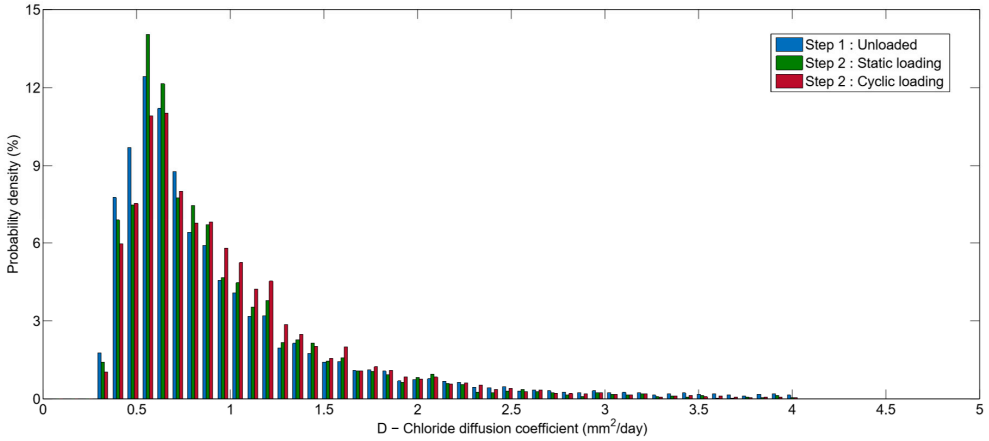

Figure 7. Comparison of a priori and a posteriori histograms of D.

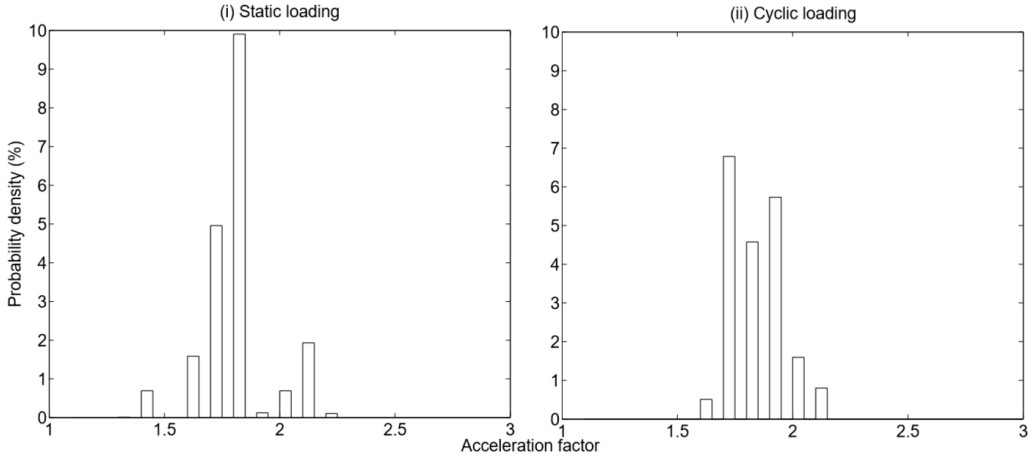

Figure 8. A posteriori histograms of α for different loadings.

The mean and standard deviation of C_s, D, and α obtained from the Bayesian networks are summarized in Table 5 for each case (without loading, static, and cyclic loading). For parameters C_s and D, the results of step 1 (without load) are very close to the values given in Table 2. It is also noted that the mean and standard deviation of C_s vary little from one loading case to another, which makes sense because all beams have been exposed to the same constant concentration of Cl^-. The parameters of D (μ and σ), are close for all cases meaning that the proposed Bayesian methodology has well separated the effects of cracking from the diffusion phenomenon which depends on the formulation and fabrication (pouring, curing, etc.) of the concrete beams. The Bayesian model allows characterization of a factor that increases the chloride diffusivity into concrete due to the presence of load-induced cracks and has a higher value for the cyclic loading. Indeed, the mean values of this factor (α) obtained from the Bayesian network are 1.73 and 1.77, respectively, for static and cyclic loading (Table 5). In both loading cases, the application of the two-step methodology makes it possible to further optimize the characterization of the parameters C_s and D by integrating the results of the tests with and without loading.

Table 5. Mean and standard deviation of a posteriori values.

	Step One		Step 2: Static Loading		Step 2: Cyclic Loading	
Parameters	**Mean**	**Standard Deviation**	**Mean**	**Standard Deviation**	**Mean**	**Standard Deviation**
C_s (% Cl^-)	0.27	0.06	0.27	0.06	0.28	0.06
D (mm^2/day)	0.94	0.66	0.94	0.57	0.95	0.58
α	-	-	1.73	0.15	1.77	0.12

5.2. Comparison with Experimental Data

50,000 Monte Carlo simulations were carried out to compute 10% and 90% percentiles and means of chloride concentrations at time t = 388 days at different measurement depths (5 mm, 15 mm, 35 mm, 35 mm). A comparison was made between the Collepardi's model (Equation (2)) with the values of Table 2, the proposed Bayesian approach with Equation (4) and the identified values (Table 5), and the experimental measurement values (Figure 9) for all loading cases. We note in Figure 9 that the 10% and 90% percentiles of the two models remain very close for all loading cases, and all points of the data fall within the 10% and 90% percentile ranges of both approaches. This indicates that the model used is complex enough to represent this experiment. Moreover, both percentiles are closer to the data for the larger depths (x = 25 or 35 mm). This is due to the fact that the model does not take into account the effects of the convection zone for depths near the surface of the concrete. This result indicates that the addition of a new random variable (α) did not significantly modify the percentiles in comparison to the Collepardi's model. This means that the proposed approach was able to distinguish between material and concrete cracking related effects and uncertainties in a comprehensive way.

Figures 10–12, compare the a posteriori histograms of the child nodes $C(x,t)$ obtained from the proposed Bayesian approach with Equation (4) and the identified values (Table 5), and those obtained from Monte Carlo simulations with Equation (2). We can see that for all the loading cases, the probability densities follow the same distributions. There is a slight difference between the densities of the BN and those of the Monte Carlo simulations, which changes with the depth and depending on the loading case. For all cases, this difference is small for the depths of x = 5 mm and 15 mm; as the depth increases, the difference between the densities more visible. In the case of static loading and for all depths, we notice that the difference decreases compared to the unloaded case; which shows that the values of the parameters C_s and D are optimized after the integration of the loaded test data. However, for cyclic loading, it increases slightly compared to the other two cases; which may be due to the relative uncertainties to the complex process of opening and closing of cracks during loading cycles. Therefore, we can conclude that the methodology allows these parameters to be updated taking into account uncertainties associated with the model and measurement methods.

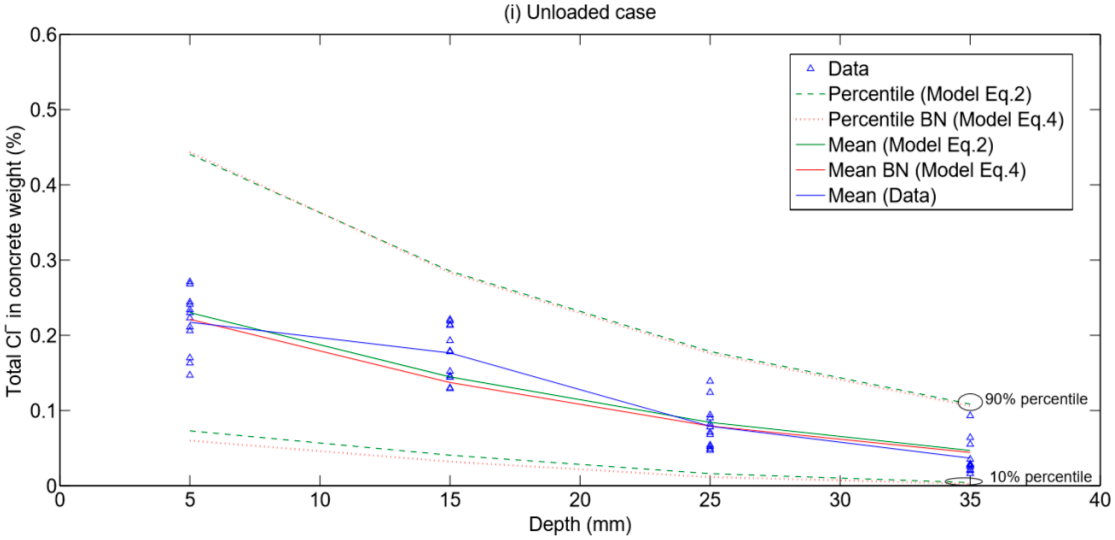

Figure 9. *Cont.*

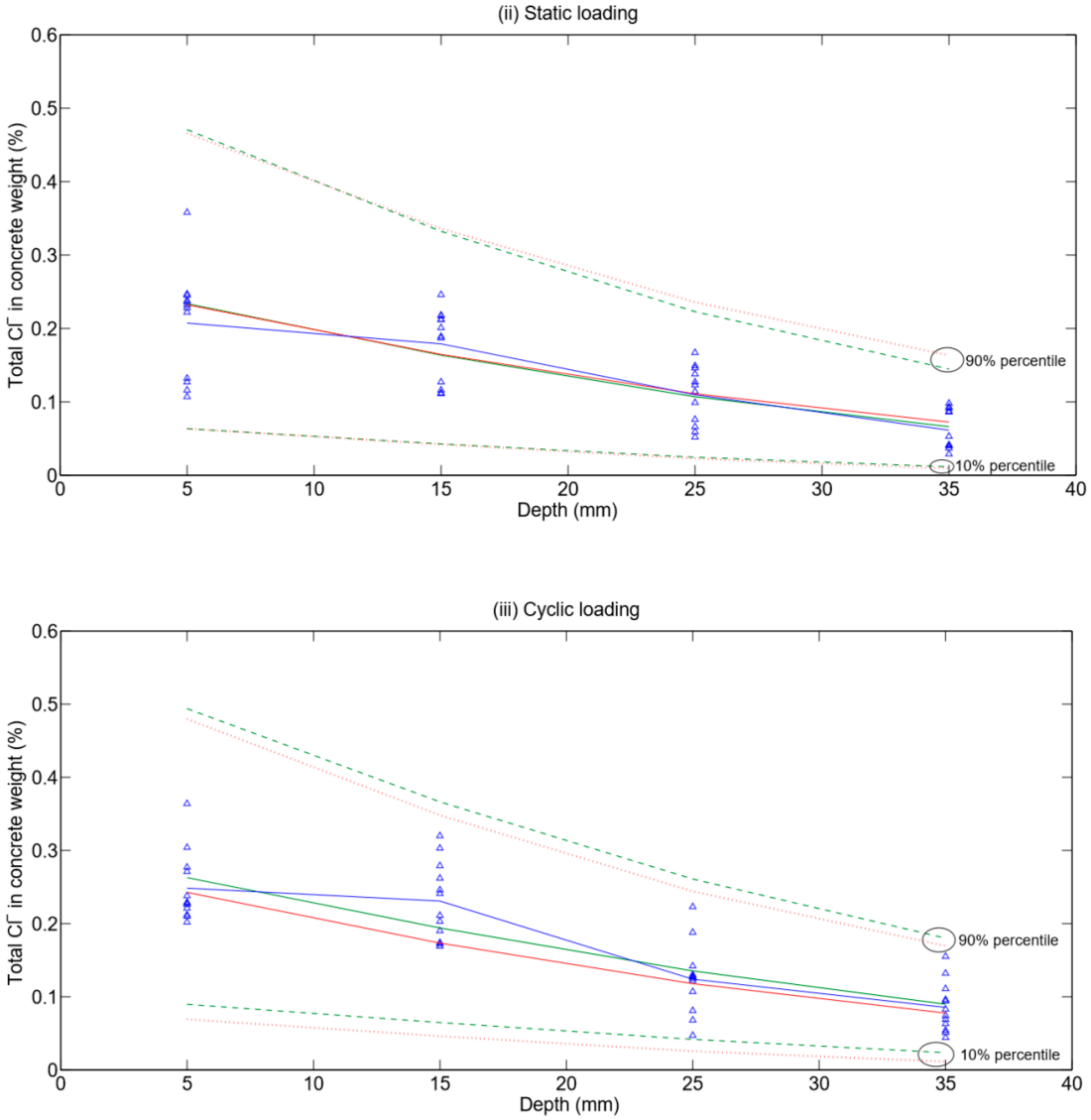

Figure 9. Comparison of chloride content into concrete at measurement depths.

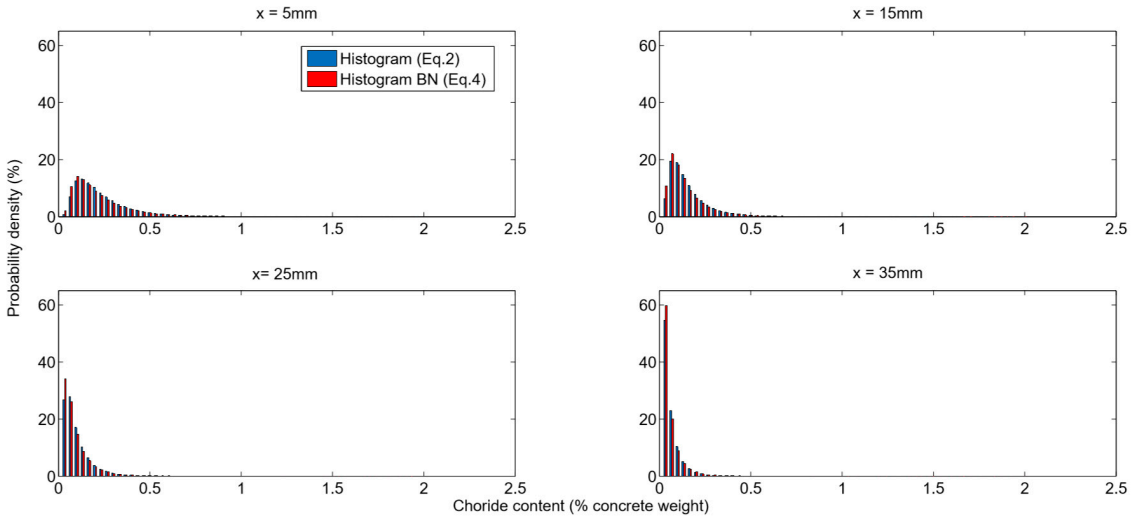

Figure 10. Distribution of chloride profiles with Equation (2) and Equation (4) for the unloaded case.

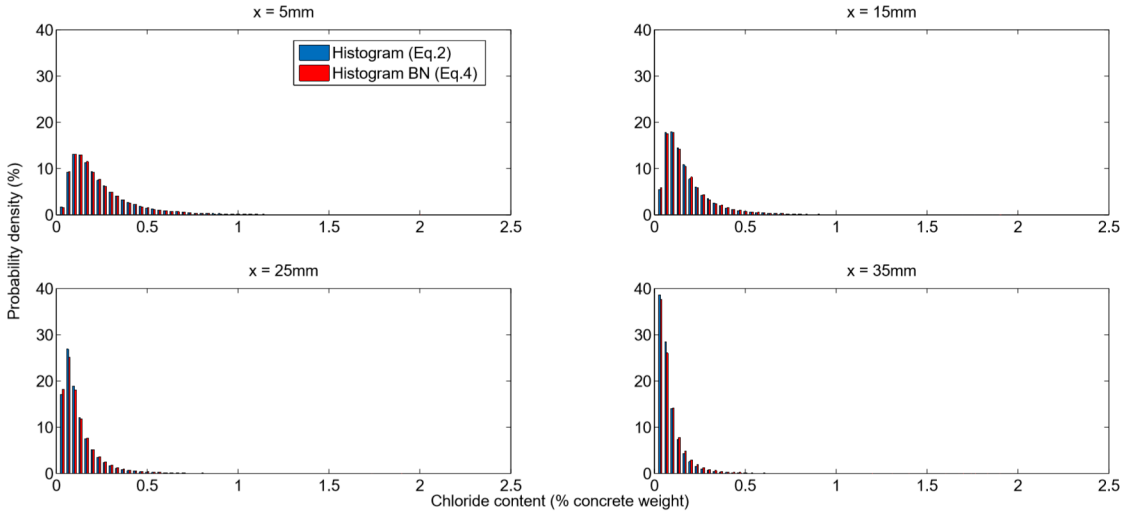

Figure 11. Distribution of chloride profiles with Equation (2) and Equation (4) percentile for the static load case.

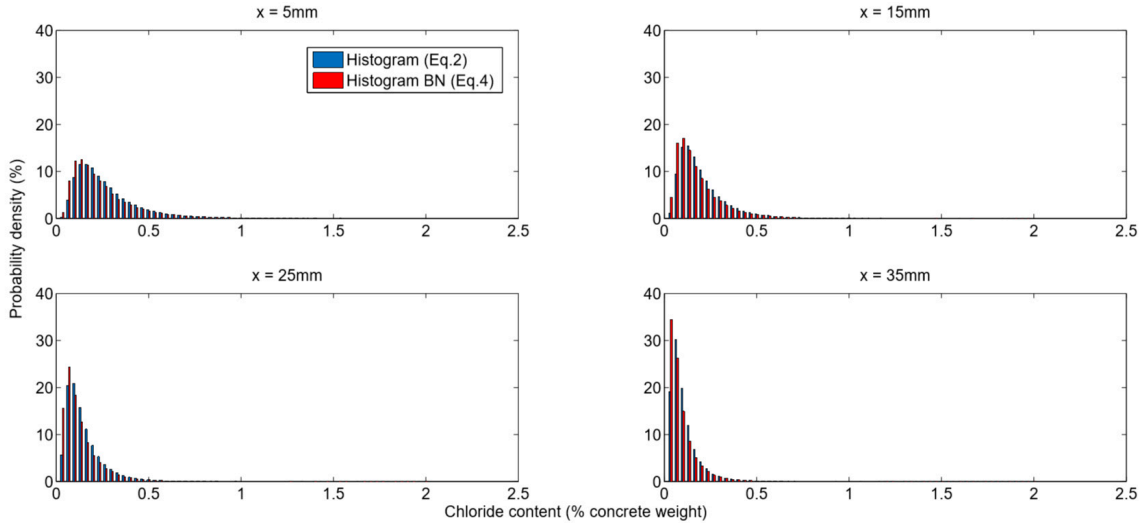

Figure 12. Distribution of chloride profiles with Equation (2) and Equation (4) percentile for the cyclic load case.

5.3. Reliability Analysis

The phenomenon of initiation to corrosion corresponds to the depassivation of steels by chloride ions. The limit state function defining corrosion initiation is written as follows:

$$g(X,t) = C_{th}(X) - C_{tc}(X,t) \tag{7}$$

where $C_{tc}(X,t)$ represents the total chloride concentration at the concrete cover depth c, at time t. This limit state function is used to estimate the probability of corrosion initiation.

5.3.1. Time of Corrosion Initiation

The corrosion initiation time t_{ini} is estimated once the chloride concentration at the cover concrete depth is equal to the threshold value C_{th} (see Equation (3)). In the case of cracked concrete, the acceleration factor α is considered in the assessment of t_{ini} as follows:

$$t_{ini} = \frac{c^2}{4\alpha D}\left[\mathrm{erf}^{-1}\left(1 - \frac{C_{th}}{C_s}\right)\right]^{-2} \tag{8}$$

Monte Carlo simulations are used to evaluate the corrosion initiation time by considering the parameters C_s, D, α and C_{th} as random variables. C_s, α and D follow log-normal distributions [32,49,50] with the mean and standard deviation given in Table 5; and C_{th} follows a uniform distribution with mean 0.4% and a coefficient of variation (COV) = 0.19% [51]. The value of the concrete cover considered is c = 40 mm and corresponds to the value considered for the design of the beams [4]. Probability density values of t_{ini}, obtained from Monte Carlo simulations for the different loading cases are given in Figure 13. It is noted that the static and cyclic loadings decrease the mean of the corrosion initiation time respectively by 1.1 and 1.31 years compared to unloaded tests. Standard deviations of corrosion initiation time are also decreased as a function of loading. These values are close to the experimental results which indicate that the mean corrosion initiation time for static and cyclic loading decreases by 1 and 1.5 years, respectively, compared to the unloaded case. Table 6 shows the mean and standard deviation values obtained with the parameters characterized for the three loading cases.

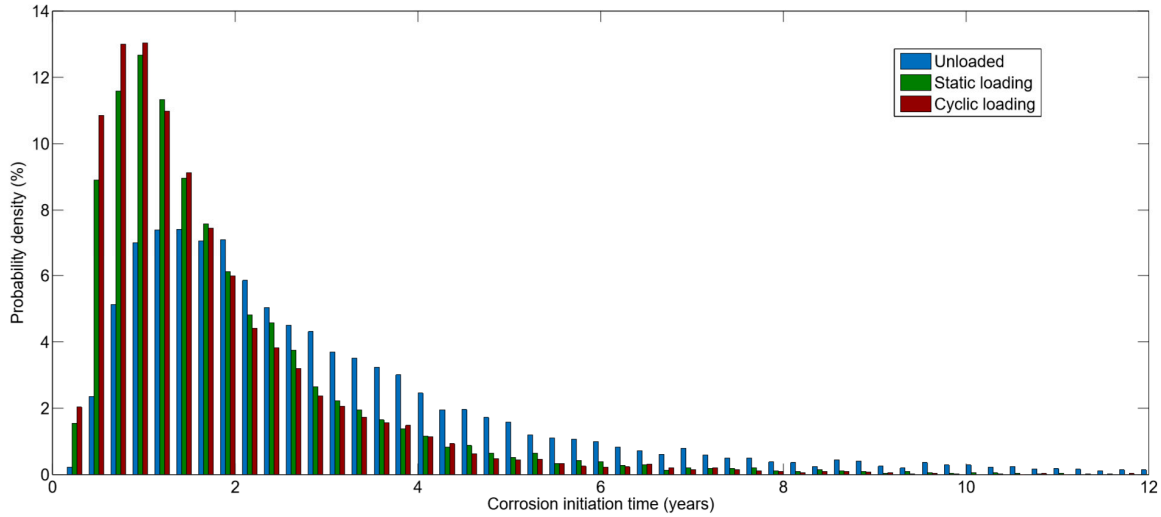

Figure 13. Probability density of corrosion initiation time.

Table 6. Mean and standard deviation of corrosion initiation time.

Case	Mean (Years)	Standard Deviation (Years)
Unloaded	2.99	2.39
Static load	1.89	1.52
Cyclic load	1.68	1.32

5.3.2. Probability of Corrosion Initiation

Figure 14 shows the corrosion initiation probability curves for the different loading cases. As expected, the probability of initiation to corrosion (PIC) increases with time and loading. This is due to the accumulation of chloride ions in the area near the reinforcements during the exposure time. Cracks in the concrete facilitate the access of oxygen and water, necessary for the oxidation reactions and the formation of rust [52]. For example, for the experimental exposure conditions, the times to reach PIC = 0.6, are 996, 575 and 505 days for, respectively, the tests without loading, with static loading and with cyclic loading. Indeed, the exposure conditions of tests are extreme because the values of the surface chloride concentration are very high [16]. The lifetime is significantly reduced for the loaded tests. These results are in agreement with experimental observations which indicate that, for certain rebars, corrosion signs have been observed at the end of the tests (t = 388 days).

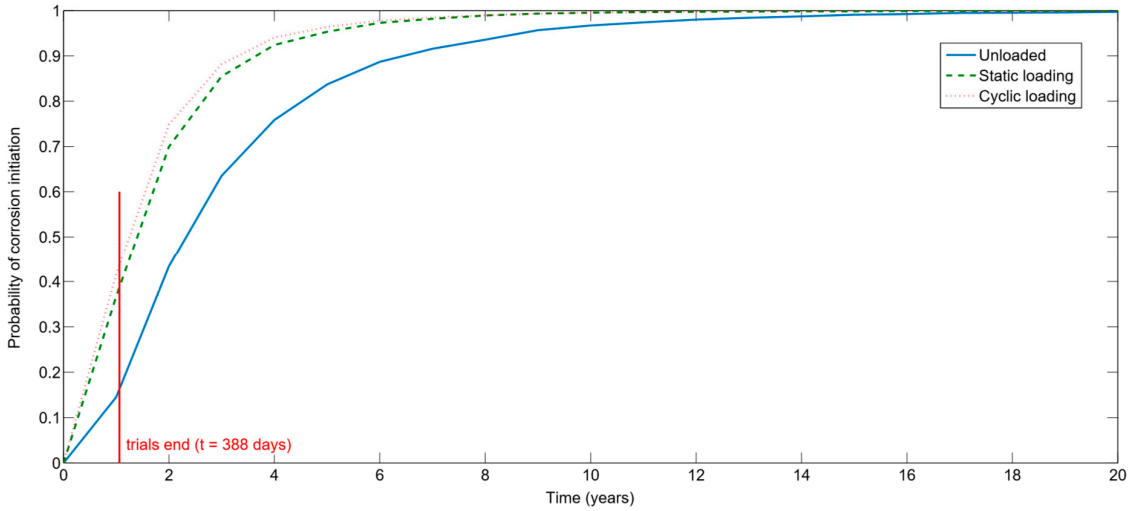

Figure 14. Probability of initiation corrosion.

6. Conclusions and Perspectives

This study proposed a methodology for the probabilistic characterization of the input parameters of a simple chlorination model including an acceleration factor for the diffusion coefficient of chloride in concrete. On the basis of the results obtained, the following conclusions are drawn:

1. The chloride content at different depths increases when the beams are loaded and for larger loading intensity.
2. The methodology, based on the Bayesian network approach, allows integrating data from experimental trials to determine the parameters of a model. It was also useful to separate the cracking effects from the diffusion of chloride ions mechanism through an acceleration factor.
3. The characterized means of the parameters C_s and D, close to the experimental values, show the usefulness of the Bayesian approach for this type of study.
4. The acceleration factor increases with the intensity of the load and is higher for the cyclic load, which resulted in larger width cracks on the beams.
5. Static and cyclic loads reduced the corrosion initiation time by 1.1 and 1.31 years, respectively, compared to the unloaded case.

In addition, one limitation of this study is the use of a simple chlorination model (Collepardi model) that does not take into account several parameters such as concrete aging and environmental conditions. Further work should consider chlorination models more representative of the chloride diffusion process. Another aspect to improve the methodology is to consider mechanics-based cracking models and to combine it with chlorination models. With these improvements, the acceleration factor could take into account crack characteristics (width, length, density, etc.), crack initiation and propagation mechanisms, and loading in a comprehensive way.

Author Contributions: Conceptualization, H.M.I., E.B.-A. and R.M.P; Data curation, X.-H.W; Funding acquisition, E.B.-A.; Methodology, H.M.I., and E.B.-A.; Software, H.M.I.; Supervision, E.B.-A., R.M.P. and S.E.A.; Validation, E.B.-A., R.M.P., S.E.A. and X.-H.W.; Writing—original draft, H.M.I.; Writing—review and editing, H.M.I., E.B.-A., R.M.P., S.E.A. and X.-H.W. All authors have read and agreed to the published version of the manuscript.

Funding: This research was funded by the Regional Council of 'Pays de la Loire' within the framework of the BUENO 2018-2021 research program (Durable Concrete for Offshore Wind Turbines).

Conflicts of Interest: The authors declare no conflict of interest.

Appendix A

Table A1. Chloride measurements for unloaded beams ($\times 10^{-2}$ concrete weight %).

	Depth (mm)			
Observations	**5**	**15**	**25**	**35**
no crack	17.0	17.9	12.4	9.30
no crack	16.3	12.9	5.40	2.70
no crack	14.7	13.0	9.00	6.40
no crack	21.1	14.4	7.10	5.50
no crack	23.0	14.6	4.90	1.60
no crack	23.4	19.3	7.80	2.80
no crack	22.3	21.3	9.40	2.70
no crack	20.6	21.4	6.80	2.10
no crack	27.1	21.9	8.20	2.50
no crack	24.1	17.8	5.20	2.90
no crack	26.8	22.1	13.9	3.50
no crack	24.4	15.2	4.70	2.00
Min	14.7	12.9	4.70	1.60
Max	27.1	22.1	13.9	9.30
μ	21.7	17.7	7.90	3.67
σ	3.99	3.54	2.93	2.27

Table A2. Chloride measurements for static loaded beams ($\times 10^{-2}$ concrete weight %).

	Depth (mm)			
Observations	**5**	**15**	**25**	**35**
one crack	12.7	11.6	7.60	3.70
one crack	13.2	11.1	6.60	4.00
one crack	10.7	12.7	5.20	2.90
one crack	11.6	11.2	5.90	4.10
one crack	23.6	21.8	12.3	4.10
one crack	23.2	20.1	9.90	4.10
one crack	35.8	21.2	13.8	5.30
two cracks	22.2	21.2	14.9	9.80
one crack	24.7	24.6	16.7	9.30
one crack	23.8	21.7	14.6	9.10
one crack	22.8	18.7	11.4	8.70
one crack	24.5	18.9	12.7	8.60
Min	10.7	11.1	5.20	2.90
Max	35.8	24.6	16.7	9.80
μ	20.7	17.9	11.0	6.14
σ	7.34	4.87	3.87	2.68

Table A3. Chloride measurements for cyclic loaded beams ($\times 10^{-2}$ concrete weight %).

	Depth (mm)			
Observations	**5**	**15**	**25**	**35**
one crack	22.6	24.1	13.0	6.90
one crack	23.8	21.1	12.5	7.40
one crack	21.0	27.9	12.7	8.30
no crack	22.1	19.0	12.2	6.30
one crack	30.4	30.3	22.3	11.10
no crack	36.4	26.2	14.2	13.2
one crack	27.7	24.6	18.8	15.5
no crack	27.1	32.0	10.7	9.60
no crack	22.8	17.2	4.70	5.10
no crack	22.9	17.4	6.80	5.40
one crack	21.2	20.3	12.8	9.40
no crack	20.2	16.9	8.10	4.40
Min	20.2	16.9	4.70	4.40
Max	36.4	32.0	22.3	15.5
μ	24.9	23.1	12.4	8.55
σ	4.76	5.23	4.81	3.39

References

1. Clifton, J.R. Predicting the service life of concrete. *ACI Mater. J.* **1993**, *90*, 611–617.
2. Jones, D.A. *Principles and Prevention of Corrosion*; Macmillan Publishing Company: New York, NY, USA, 1992.
3. Virmani, Y.P. *Corrosion Costs and Preventive Strategies in the United States*; US Department of Transportation: Philadelphia, PA, USA, 2002; pp. 1–16.
4. Wang, X.-H.; Bastidas-Arteaga, E.; Gao, Y. Probabilistic analysis of chloride penetration in reinforced concrete subjected to pre-exposure static and fatigue loading and wetting-drying cycles. *Eng. Fail. Anal.* **2018**, *84*, 205–219. [CrossRef]
5. Bastidas-Arteaga, E.; Schoefs, F. Sustainable Maintenance and Repair of RC Coastal Structures. *Proc. ICE-Marit. Eng.* **2015**, *168*, 162–173. [CrossRef]
6. Bastidas-Arteaga, E.; Schoefs, F.; Chateauneuf, A.; Sánchez-Silva, M.; Capra, B. Probabilistic Evaluation of the Sustainability of Maintenance Strategies for RC Structures Exposed to Chloride Ingress. *Int. J. Eng. Uncertain. Hazards Assess. Mitig.* **2010**, *2*, 61–74.
7. Poupard, O.; L'Hostis, V.; Catinaud, S.; Petre-Lazar, I. Corrosion damage diagnosis of a reinforced concrete beam after 40 years natural exposure in marine environment. *Cem. Concr. Res.* **2006**, *36*, 504–520. [CrossRef]
8. Mehta, P.K. Durability—Critical Issues for the Future. *Concr. Int.* **1997**, *19*, 27–33.
9. Djerbi, A.; Bonnet, S.; Khelidj, A.; Baroghel-bouny, V. Influence of traversing crack on chloride diffusion into concrete. *Cem. Concr. Res.* **2008**, *38*, 877–883. [CrossRef]
10. Saito, M.; Ishimori, H. Chloride permeability of concrete under static and repeated compressive loading. *Cem. Concr. Res.* **1995**, *25*, 803–808. [CrossRef]
11. Sadowski, L. Non-destructive investigation of corrosion current density in steel reinforced concrete by artificial neural networks. *Arch. Civ. Mech. Eng.* **2013**, *13*, 104–111. [CrossRef]
12. Golewski, G.L. Measurement of fracture mechanics parameters of concrete containing fly ash thanks to use of Digital Image Correlation (DIC) method. *Measurement* **2019**, *135*, 96–105. [CrossRef]
13. Niewiadomski, P.; Hoła, J. Failure process of compressed self-compacting concrete modified with nanoparticles assessed by acoustic emission method. *Autom. Constr.* **2020**, *112*, 103111. [CrossRef]
14. Sadowski, Ł.; Hoła, J.; Czarnecki, S. Non-destructive neural identification of the bond between concrete layers in existing elements. *Constr. Build. Mater.* **2016**, *127*, 49–58. [CrossRef]
15. Golewski, G.L. Estimation of the optimum content of fly ash in concrete composite based on the analysis of fracture toughness tests using various measuring systems. *Constr. Build. Mater.* **2019**, *213*, 142–155. [CrossRef]

16. Bastidas-Arteaga, E.; Bressolette, P.; Chateauneuf, A.; Sánchez-Silva, M. Probabilistic lifetime assessment of RC structures under coupled corrosion–fatigue deterioration processes. *Struct. Saf.* **2009**, *31*, 84–96. [CrossRef]
17. Bastidas-Arteaga, E. Reliability of Reinforced Concrete Structures Subjected to Corrosion-Fatigue and Climate Change. *Int. J. Concr. Struct. Mater.* **2018**, *12*, 10. [CrossRef]
18. Chapter 26 Environmental Cracking Corrosion Fatigue. Available online: https://www.astm.org/DIGITAL_LIBRARY/MNL/PAGES/MNL11032M.htm (accessed on 27 July 2019).
19. Giordano, L.; Mancini, G.; Tondolo, F. Reinforced Concrete Members Subjected to Cyclic Tension and Corrosion. *J. Adv. Concr. Technol.* **2011**, *9*, 277–285. [CrossRef]
20. Boulfiza, M.; Sakai, K.; Banthia, N.; Yoshida, H. Prediction of Chloride Ions Ingress in Uncracked and Cracked Concrete. *Mater. J.* **2003**, *100*, 38–48.
21. Wang, X.-H.; Gao, Y.; Gao, R.-D.; Wang, J.; Liu, X.-L. Influence of different fatigue loads and coating thicknesses on service performance of RC beam specimens with epoxy-coated reinforcement. *Comput. Concr.* **2017**, *19*, 243–256. [CrossRef]
22. Saassouh, B.; Lounis, Z. Probabilistic modeling of chloride-induced corrosion in concrete structures using first- and second-order reliability methods. *Cem. Concr. Compos.* **2012**, *34*, 1082–1093. [CrossRef]
23. Bentz, E.C. Probabilistic Modeling of Service Life for Structures Subjected to Chlorides. *Mater. J.* **2003**, *100*, 391–397.
24. Schoefs, F.; Bastidas-Arteaga, E.; Tran, T.V.; Villain, G.; Derobert, X. Characterization of random fields from NDT measurements: A two stages procedure. *Eng. Struct.* **2016**, *111*, 312–322. [CrossRef]
25. Nogueira, C.G.; Leonel, E.D. Probabilistic models applied to safety assessment of reinforced concrete structures subjected to chloride ingress. *Eng. Fail. Anal.* **2013**, *31*, 76–89. [CrossRef]
26. Tuutti, K. *Corrosion of Steel in Concrete*; Cement-och Betonginst.: Stockholm, Sweden, 1982; p. 468.
27. Bastidas-Arteaga, E.; Schoefs, F.; Bonnet, S.; O'Connor, A. Bayesian identification of uncertainties in chloride ingress modeling into reinforced concrete structures. In Proceedings of the Third International Symposium on Life-Cycle Civil Engineering, Vienna, Austria, 3–6 October 2012.
28. Richard, B.; Adelaide, L.; Cremona, C. A Bayesian approach to estimate material properties from global statistical data. *Eur. J. Environ. Civ. Eng.* **2012**, *16*, 460–470. [CrossRef]
29. Tran, T.-B.; Bastidas-Arteaga, E.; Aoues, Y.; Pambou Nziengui, C.F.; Hamdi, S.E.; Moutou Pitti, R.; Fournely, E.; Schoefs, F.; Chateauneuf, A. Reliability assessment and updating of notched timber components subjected to environmental and mechanical loading. *Eng. Struct.* **2018**, *166*, 107–116. [CrossRef]
30. Tran, T.-B.; Bastidas-Arteaga, E.; Aoues, Y. A Dynamic Bayesian Network framework for spatial deterioration modelling and reliability updating of timber structures subjected to decay. *Eng. Struct.* **2020**, *209*, 110301. [CrossRef]
31. Stewart, M.G.; Rosowsky, D.V. Time-dependent reliability of deteriorating reinforced concrete bridge decks. *Struct. Saf.* **1998**, *20*, 91–109. [CrossRef]
32. Saetta, A.V.; Scotta, R.V.; Vitaliani, R.V. Analysis of Chloride Diffusion into Partially Saturated Concrete. *Mater. J.* **1993**, *90*, 441–451.
33. Nguyen, P.T.; Bastidas-Arteaga, E.; Amiri, O.; El Soueidy, C.-P. An Efficient Chloride Ingress Model for Long-Term Lifetime Assessment of Reinforced Concrete Structures under Realistic Climate and Exposure Conditions. *Int. J. Concr. Struct. Mater.* **2017**, *11*, 199–213. [CrossRef]
34. Otieno, M.; Beushausen, H.; Alexander, M. Chloride-induced corrosion of steel in cracked concrete—Part II: Corrosion rate prediction models. *Cem. Concr. Res.* **2016**, *79*, 386–394. [CrossRef]
35. Gowripalan, N.; Sirivivatnanon, V.; Lim, C.C. Chloride diffusivity of concrete cracked in flexure. *Cem. Concr. Res.* **2000**, *30*, 725–730. [CrossRef]
36. Otieno, M.; Beushausen, H.; Alexander, M. Towards incorporating the influence of cover cracking on steel corrosion in RC design codes: The concept of performance-based crack width limits. *Mater. Struct.* **2012**, *45*, 1805–1816. [CrossRef]
37. Kurumatani, M.; Anzo, H.; Kobayashi, K.; Okazaki, S.; Hirose, S. Damage model for simulating chloride concentration in reinforced concrete with internal cracks. *Cem. Concr. Compos.* **2017**, *84*, 62–73. [CrossRef]
38. Du, X.; Jin, L.; Zhang, R.; Li, Y. Effect of cracks on concrete diffusivity: A meso-scale numerical study. *Ocean Eng.* **2015**, *108*, 539–551. [CrossRef]

39. Peng, J.; Hu, S.; Zhang, J.; Cai, C.S.; Li, L. Influence of cracks on chloride diffusivity in concrete: A five-phase mesoscale model approach. *Constr. Build. Mater.* **2019**, *197*, 587–596. [CrossRef]
40. Wang, L.; Bao, J.; Ueda, T. Prediction of mass transport in cracked-unsaturated concrete by mesoscale lattice model. *Ocean Eng.* **2016**, *127*, 144–157. [CrossRef]
41. Gjørv, O.E. Durability of reinforced concrete wharves in Norwegian harbours. *Mater. Constr.* **1969**, *2*, 467–476. [CrossRef]
42. Win, P.P.; Watanabe, M.; Machida, A. Penetration profile of chloride ion in cracked reinforced concrete. *Cem. Concr. Res.* **2004**, *34*, 1073–1079. [CrossRef]
43. Lindquist, W.D.; Darwin, D.; Browning, J.; Miller, G.G. Effect of Cracking on Chloride Content in Concrete Bridge Decks. *ACI Mater. J.* **2006**, *103*, 467–473.
44. GB/T 50081-2016. *Standard for Test Method of Mechanical Properties on Ordinary Concrete*; National Standard of the People's Republic of China: Beijing, China, 2016.
45. GB50010-2010. *Code for Design of Concrete Structures*; National Standard of the People's Republic of China: Beijing, China, 2010.
46. Wang, X.-H.; Chen, B.; Gao, Y.; Wang, J.; Gao, L. Influence of external loading and loading type on corrosion behavior of RC beams with epoxy-coated reinforcements. *Constr. Build. Mater.* **2015**, *93*, 746–765. [CrossRef]
47. Wang, X.-H.; Gao, Y. Corrosion behavior of epoxy-coated reinforced bars in RC test specimens subjected to pre-exposure loading and wetting-drying cycles. *Constr. Build. Mater.* **2016**, *119*, 185–205. [CrossRef]
48. Holmes, D.E.; Jain, L.C. *Innovations in Bayesian Networks*; Springer: Berlin/Heidelberg, Germany, 2008.
49. Bastidas-Arteaga, E.; Stewart, M.G. Economic assessment of climate adaptation strategies for existing reinforced concrete structures subjected to chloride-induced corrosion. *Struct. Infrastruct. Eng.* **2016**, *12*, 432–449. [CrossRef]
50. Vu, K.A.T.; Stewart, M.G. Structural reliability of concrete bridges including improved chloride-induced corrosion models. *Struct. Saf.* **2000**, *22*, 313–333. [CrossRef]
51. Comité Européen de Normalisation (CEN). *Concrete—Part 1: Specification, Performance, Production and Conformity*; Comité Européen de Normalisation: Brussels, Belgium, 2000.
52. Papakonstantinou, K.G.; Shinozuka, M. Probabilistic model for steel corrosion in reinforced concrete structures of large dimensions considering crack effects. *Eng. Struct.* **2013**, *57*, 306–326. [CrossRef]